Effect of Inclined Wall Plan Jet Flow Issued in a Main Flow

F. Sh. Abou-Taleb* and A. Abdel- Fattah**
* Lecturer, ****Associate Professor, Department of Mechanical Power Engineering, Faculty of Engineering Menoufia University, Shebin El-Kom, Egypt.**

fauzy1957@yahoo.com
ashourabdelfatah@yahoo.com

Abstract

In this paper, the numerical and experimental results for the effect of the velocity ratio and the jet angle on the flow field for inclined jet into cross flow have been studied. Experiments were done at velocity ratios between the jet and main flow from 5.8 to 20.5 and from 0.1 to 25.5 in numerical study. The angle between the jet and the main flow direction was 30^o, 60^o and 90^o. The numerical study is based on the solution of the complete Navier – Stokes equations using and the k- ε turbulence model with Schziiner and Rodi correction by a finite method ... The results show that, the size of recirculation zone after jet increases as the velocity ratio increases and increases with the jet angle increase. The wall pressure increases to reach maximum value and then decreases to reach a minimum value after the jet location in the recirculation zone then increases again reaching the atmospheric at the exit. The results also indicated that the reattachment length increases by increasing of velocity ratio and / or increasing the jet angle. At low and moderate values of velocity ratio (0.1 and 0.8), the numerical results were compared with measurement data [1]. Also the comparisons give a good agreements for the predicted static pressure and velocity distribution compared with the experimental one for the tested cases.
Keywords: cross flow, recirculation zone, turbulence model

البحث يحتوى على دراسة عملية ونظرية لدراسة تأثير نسبة السرعة (سرعة نفث مائل الى سرعة سريان رئيسى أفقى) وكذلك زاوية ميل النفث على شكل السريان . **التجارب المعملية تمت عند نسب سرعات من ٥.٨ الى ٢٠.٥ وعند زوايا ميل ٣٠،٦٠، و٩٠ درجة وأما الدراسة النظرية تمت تنسب سرعات من ٠.١ حتى ٢٥.٥. تعتمد الدراسة النظرية على حل معادلات** Navier – Stokes **مستخدما موديل** k- ε **بطريقة رودى وشيزنر وتم حل هذة المعادلات مستخدما الفروق الحجمية . النتائج النظرية المستخلصة أظهرت ان حجم منطقة الدوامات بعد النفثص تزداد نتيجة زيادة نسبة السرعة وزاوية ميل النفث. الضغط الأستاتيكى على الحائط يزداد ليصل أقصى قيمة ثم يقل لأقل قيمة بعد النفث فى منطقة الدوامات ثم يزداد ثانية حتى يصل الى الضغط الجوى. النتائج أظهرت أيضا ان الطول يزداد بزيادة نسبة السرعة او زاوية ميل النفث. عند قيم صغيرة ومتوسطة لنسبة السرعة (٠.١ – ٠.٨) قورنت مع قياسات [١] وكانت النتائج متوافقة مع كل حالات الدراسة.وعقدت عدة مقارنات بين النتائج النظرية والنتائج العملية لآخرين لتوزيع السرعة والضغط الأستاتيكى وأظهرت تلك المقارنات توافقا جيدا.**

Introduction

The flow from holes and slot into cross flow is used in various applications, such as, turbine blade cooling, effluent discharged into the atmosphere and waste discharge into rivers.

In recent studies, Fitt et al.[1] studied experimentally the injection flow for a 90^o slot into a cross flow with different values of velocity ratio. Ramaprian and Haniu [2]

studied experimentally, the turbulent plane non- buoyant isothermal and heated jets in a cross flow for jet to stream velocity ratio (R) 6, 9 and 10. They measure the mean velocity components and their fluctuation as well as mean temperatures. Also they reported the measurements of mean and turbulent quantities for the case of buoyant jets for the same configurations [3]. Barata et al. [4] and Barata [5],studied the velocity characteristics of multiple impinging jets through a cross flow in [4],and fountain flows produced by multiple impinging jets in cross flow [5]. Their results showed the presence of complex three dimensional scarf vortex formed around each impinging jet and fountain up mass flow resulting from the collision of the wall jets. The injection of cold jet stream in a strong cross flow ($R \leq 1$) of hot fluid indicated by Sarkar and Bose [6]. Launder and Spalding [7] used the k-ε standard model to simulate the turbulent round jets in cross flow. Patankar et al. [8], Catalano et al.[9], He et al.[10] have produced round turbulent jets in weak and moderate cross flow ($R \geq 2$). The aerodynamics of a two dimensional slot cooling geometry studied numerically by Kassimatis et al. [11].They indicated the wall pressure and the velocity function of the injection ratio. Their results showed that the pressure increases to reach maximum value and it decreases suddenly after the injection position. Also the reattachment length increases as the injection ratio increases. The comparison between of Yang- Shih and standard k- ε turbulence models for impingement jet in cross flow was studied by El-Gabry and Kaminski [12]. They showed that the standard k- ε turbulence model is better at high Reynolds number and it is not possible to conclude that one turbulence model is more accurate than another. Kalita et al.[13] studied numerically the turbulent plane jet in cross flow. They used the standard k-ε model to formulate the flow problem. Their results show the effect of velocity ratio (R = 6, 9 and 10) on the mean velocity and the fluctuation of the velocity.

From the previous discussion of the literature review, it can be concluded that, the work dearly with the effect of the jet angle and the higher velocity ratio on the cross flow is little. In this paper, the effect of the jet angle and the velocity ratio on the mean flow vector fields, the velocity components and the wall pressure are studied numerically and experimentally.

2. EXPERIMENTAL SETUP

A suction subsonic open type wind tunnel is used in this work to derive the main flow. The air flows through a honeycomb and an air filter to the contraction nozzle, then to the test section. The test section is a rectangular cross section 4 cm width,30cm height and 60 cm long made of prespex(fig.1a). The air then flows to a divergent section through a variable speed fan to out side. The velocity can be varied from 5 to 55 m/sec. A jet of air is issued to the test section trough a slot of 1 cm width inclined to the horizontal at three inclination angle $\theta = 30, 60$ and 90^{o} located at the front of the lower surface of the test section. The air jet is issued to the test section from a reservoir of a maximum pressure of 8 bar charged to two reciprocating compressors. A control valve installed in the pipe connected to the slot is used with the help of regulating switch of the wind tunnel, to obtain the desired velocity ratio(5.8 , 15.2 and 20.5).

A two dimensional traverse mechanism is supported on the top surface of the test section holds a prob for measurements of the velocity in the test section. Pressure taps located along the lower surface of the test section connected to multiple water u-tube manometers used to measure the static pressure distributions.

3. MATHEMATICAL MODELS

The physical model used in this study is shown in Figure 1b . The test section is a rectangular cross section (height *H* and width *b*). Plane jet of air is issuing from slot with a wide equal the width of the test section.

The inlet velocity of jet V_J and U_C of main flow are uniform. To facilitate the analysis, the following assumptions are made.

The fluid is air and the flow field is two dimensional, incompressible and turbulent

Based on the characteristics scales of *b*, V_J, the dimensionless variables are defined as follows.

$$x = \frac{\bar{x}}{b}\ ,\quad y = \frac{\bar{y}}{b},\quad u = \frac{\bar{u}}{V_J},\quad v = \frac{\bar{v}}{V_J},\qquad p = \frac{\bar{p}}{\rho V_J^2}$$

Where the over bar represents the dimensional quantities. According to the above assumptions and dimensionless variables, the dimensionless governing equations are expressed as the following equations.

Continuity equation

$$\frac{\partial u}{\partial x} + \frac{\partial v}{\partial y} = 0 \tag{1}$$

Momentum equations:

$$u\frac{\partial u}{\partial x} + v\frac{\partial u}{\partial y} = -\frac{\partial p}{\partial x} + \frac{\partial}{\partial x}\left(\frac{1}{\mathrm{Re}}\right) + \frac{1}{\mathrm{Re}_t}\frac{\partial u}{\partial x}\Big] + \frac{\partial}{\partial y}\left(\frac{1}{\mathrm{Re}}\right) + \frac{1}{\mathrm{Re}_t}\frac{\partial u}{\partial y}\Big]$$
$$+ \frac{\partial}{\partial x}\left(\frac{1}{\mathrm{Re}_t}\frac{\partial u}{\partial x}\right) + \frac{\partial}{\partial y}\left(\frac{1}{\mathrm{Re}_t}\frac{\partial v}{\partial x}\right) \tag{2}$$

$$u\frac{\partial v}{\partial x} + v\frac{\partial v}{\partial y} = -\frac{\partial p}{\partial y} + \frac{\partial}{\partial x}\left(\frac{1}{\mathrm{Re}}\right) + \frac{1}{\mathrm{Re}_t}\frac{\partial v}{\partial x}\Big] + \frac{\partial}{\partial y}\left(\frac{1}{\mathrm{Re}}\right) + \frac{1}{\mathrm{Re}_t}\frac{\partial v}{\partial y}\Big]$$
$$+ \frac{\partial}{\partial x}\left(\frac{1}{\mathrm{Re}_t}\frac{\partial u}{\partial y}\right) + \frac{\partial}{\partial y}\left(\frac{1}{\mathrm{Re}_t}\frac{\partial v}{\partial y}\right) \tag{3}$$

The transport equations for turbulent kinetic energy and its dissipation are given by:

$$u\frac{\partial k}{\partial x} + v\frac{\partial k}{\partial y} = \frac{\partial}{\partial x}\left(\frac{1}{\mathrm{Re}}\right) + \frac{1}{s_k\ \mathrm{Re}_t}\frac{\partial k}{\partial x}\Big] + \frac{\partial}{\partial y}\left(\frac{1}{\mathrm{Re}}\right) + \frac{1}{s_k\ \mathrm{Re}_t}\frac{\partial k}{\partial y}\Big] + G - e \tag{4}$$

$$u\frac{\partial e}{\partial x}+v\frac{\partial e}{\partial y}=\frac{\partial}{\partial x}\left[\left(\frac{1}{\mathrm{Re}}+\frac{1}{s_e\,\mathrm{Re}_t}\right)\frac{\partial e}{\partial x}\right]+\frac{\partial}{\partial y}\left[\left(\frac{1}{\mathrm{Re}}+\frac{1}{s_e\,\mathrm{Re}_t}\right)\frac{\partial e}{\partial y}\right]+c_1\frac{e}{k}G-c_2\frac{e^2}{k} \quad (5)$$

Where G is the rate of production of k and is given by

$$G=\frac{1}{\mathrm{Re}_t}\left[\left(\frac{\partial u}{\partial y}+\frac{\partial v}{\partial x}\right)^2+2\left(\frac{\partial u}{\partial x}\right)^2+2\left(\frac{\partial v}{\partial y}\right)^2\right] \quad (6)$$

Where

Re_t is the turbulent Reynolds number and it can be calculated by

$Re_t = \rho V_J\, b/\mu_t$

The turbulent viscosity is calculated from this relation,

$$\mu_t = c_m\frac{\rho\, k^2}{\varepsilon}$$

Here μ_t is the eddy viscosity, c_μ is a model constant, k is the turbulent kinetic energy, and ε is the dissipation rate of the turbulent kinetic energy.

Leschziner and Rodi [14] incorporated the effects of stream line curvature on c_μ in the form.

$$c_m = Max\left[0.025,\frac{0.09}{1+0.57\frac{k^2}{\varepsilon^2}\left(\frac{\partial V_{tot}}{\partial n}+\frac{V_{tot}}{R_c}\right)\frac{V_{tot}}{R_c}}\right] \quad (7)$$

The curvature radius R_c is given from

$$\frac{1}{R_c}=\frac{uv\left(\frac{\partial v}{\partial y}-\frac{\partial u}{\partial x}\right)+u^2\frac{\partial v}{\partial x}-v^2\frac{\partial u}{\partial y}}{\left(u^2+v^2\right)^{1.5}} \quad (8)$$

The values of the model constants are taken as:

c_1 =1.44 , c_2 = 1.92, c_3 = 1.373, σ_k= 1 and σ_ε =1.3

The computational domain boundaries are shown in figure 2(a)

The boundary conditions for the above set of governing equations are as follows:

a) Inlet boundary (a-b, c-d)

The uniform velocity, turbulent kinetic energy and dissipation rate are

at (a-b) i-e, u = U_c, $k_c = 0.04U_c$ and $\varepsilon_c = \frac{c_\mu k_c^{1.5}}{0.1H}$

at (c-d) i-e, $v = V_J$, $k_J = 0.001V_J$ and $\varepsilon_J = \frac{c_\mu k_J^{1.5}}{0.1b}$

b) at walls (b-c, d-e and f-a)

The condition at solid wall are imposed $u = v = 0$. In the standard k- ε model and the velocity at the grids adjacent to wall are specified by wall function. The wall function are suggested by Launder and Spalding [7]

d) Exit boundary

A zero gradient condition is employed across the outlet boundary. Although this boundary condition is strictly valid only when flow is fully developed, it is also permissible for sufficient downstream from the region of interest, i.e., $\frac{\partial f}{\partial y} = 0$ and $\phi = u,\ v,\ k$ and ε

4. SOLUTION PROCEDURE

The governing differential equations for mass, momentum, energy, turbulent kinetic energy and its dissipation rate were solved using the control-volume-based finite difference method described by Patankar [15]. The SIMPLE algorithm [15] was used to resolve the pressure- velocity coupling. A 121 x 61 grid was placed non-uniformly in the computational domain. The x direction (stream wise) grids were chosen non-uniform, front and behind of jet inlet. The grids were expanded by power low formulation with a power of 0.95, from in jet center to two sides; front even the inlet cross flow and behind even the distance equal the distance between the jet center and the inlet cross flow, and the grids remain with constant value until the outlet section of flow. The y direction grid was chosen non-uniform, such that the finest grid was in side of wall jet and was expanded out word by power low formulation with a power of 1.01, see figure 2(a). The effect of the turbulence correction using by Leschziner and Rodi [14] to calculate the eddy viscosity on the x-component velocity (u / Uc) is shown in figure 2(b).

5. RESULTS AND DISCUSSION

5.1. The mean Flow vector fields

Figure 3(a-d) shows the mean velocity vector fields at different values of velocity ratio (R) and constant value of jet angle ($\theta = 90^o$). This velocity ratio was varying from low ratio (R = 0.1) in figure 3a, moderate velocity ratio(R=0.8) in figure 3b, high velocity ratio(R = 15.2) in figure 3(c) and highest value of velocity ratio(R = 20.5) in figure 3(d). From this figure, it can be seen that, the recirculation zone was generated behind the injection location. This is because the injection flow restricts the main flow in the injection side of the test section. As the velocity ratio increases, this zone increases, see figure 3b. At high values of velocity ratio the recirculation zone generated upstream the jet due to the deflection of the streamline of the main flow far away of injection location see figure 3(c). From figure 3(d), it is observed that, at highest values of velocity ratio (R = 20.5) the recirculation zones which generated upstream and downstream the jet increase consequently, the reattachment length increases. Also it can be seen that, the amount of penetration of the jet into the cross flow and the deflection of the streamlines depend on the value of the velocity ratio. The effect of jet angle on the mean velocity vector fields is shown in figure 4(a-c). From this figure it can also noticed that, when the jet angle decreases, the

recirculation zones decrease. This is due to the horizontal component (u) at inlet of jet, this component increases by decreasing of the jet angle.
Finally, the injection in cross flow is generally has similar effect as the obstacle in main flow, the intensity of the jet represents the height of obstacle. If the intensity of injection increases, the intensity of secondary flow increases.

5.2 Effect of x distance on the x-component velocity.

Figure 5 shows the dimensionless of the horizontal component of local mean velocity (u/ Uc) variation with changing the dimensionless vertical distance (y/b) at different values of the dimensionless distance x/b within the separated region. From this figure, it can be seen that the velocity changed from zero value at the injection wall and becomes negative value reaches to minimum value, then increases to reach the positive value and it decreases with increase the vertical distance. At the distance x/b is 9, the negative velocity is big value in the separation zone and it decreases at higher value of distance. This is because the vorticity increases..

5.3 Effect of velocity ratio on the x-component velocity.

Figure 6 represents a graph of the dimensionless of the horizontal component of local mean velocity (u/ Uc) as a function of the dimensionless vertical distance (y/b) , a fixed jet angle ($\theta = 90^o$) and a fixed dimensionless distance x/b (x/b= 19)for three different velocity ratios. From this figure, it can be observed that, as the velocity ratio increases, the negative velocity in the separation zone increases. This is because the vorticity increases in this zone by increasing the velocity ratio. As, the velocity ratio increases, the maximum positive value increases, this is because the width of the recirculation zone increases consequently, the area of main flow decreases so the velocity increases. Also, the velocity from maximum positive value becomes approximately constant with increase the vertical velocity.

5.4 Effect of jet angle on the x-component velocity

Figure 7 illustrates, the change in the dimensionless horizontal component of velocity (u/ Uc) with dimensionless vertical distance (y/b), at different value of jet angle ($\theta = 30^o$, 60^o and 90^o) at fixed dimensionless distance (x/b= 9). From this figure, it can be seen that, at higher value of jet angle ($\theta = 90^o$), the negative value of the velocity is bigger and decreases by decreasing the jet angle. The negative velocity in the recirculation zone decreases by decreasing the jet angle and it becomes positive value at jet angle equal 30^o. This is because the intensity of the secondary flow is bigger at angle 90^o. But for the jet angle is 60^o, the injection flow has horizontal component at jet inlet, this component reduces the recirculation zone, and then the secondary flow in this zone decreases. At the jet angle ofl 30^o, this component at jet inlet becomes bigger than the vertical component for the injection term, and then the recirculation zone is not found behind the jet for this angle.

5.5 Effect of turbulence model on the x-component velocity

Figure 8(a-f) shows the effect of turbulence model on the dimensionless horizontal component of velocity profile (u/ Uc), for two different values of velocity ratios (R = 0.1 and 0.8) , and fixed jet angle ($\theta = 90^o$) and different values of dimensionless distance x/b. From this figure, it can be seen that, the k- ε model with Leschziner and Rodi [14] correction is better than the standard k- ε model. Also it can be noticed that,

the comparison between the numerical results and experimental data [1] gives good agreements.

5.6 The y-component velocity profiles.

The vertical dimensionless velocity distributions $(v/U_c)(y/b)$ at different sections, jet angle $\theta = 90^o$, and velocity ratio R=20.5 are shown in figure 9. From this figure, it can be seen that, generally, the trend is same for all cases of distance x/b, the velocity decreases from the down wall of test section to reach a minimum value and it increases to reach maximum value in the upper half test section then decreases to reach zero value at the upper wall. The negative value of the vertical velocity (v/U_c) decreases by increasing the distance x/b. The absolute value of this velocity in the down half of test section is higher than that in the upper half test section. This due to the decay of the x-component velocity in the down half test section. The effect of the velocity ratio on the vertical velocity profile is quite clear in figure 10 .The negative value of this velocity increases as the velocity ratio increases. The results for different values of jet angle are shown in figure 11. From this figure, it is seen that, the minimum value of this velocity which occurs in the recirculation zone behind the jet location changes the sign and it becomes maximum value at jet angle equal 60^o. The maximum value of this velocity is higher and shifts toward the upper wall at jet angle equal 30^o than at jet angle equal 60^o. Generally this component depends on the distributions of the horizontal velocity

5.7 Effect of velocity ratio on the wall pressure distributions

In figure 12(a-d), the effect of the velocity ratio (R) on the wall pressure coefficient $(\overline{P}_w - \overline{p}_a / 0.5rU_c^2)$£ at constant value of jet angle is presented. From this figure, it can be seen that, the trend is same for all cases of velocity ratio. The pressure increases front the jet to peak value due to the presence of the injection, then the pressure decreases quickly to minimum value because the jet flow restricts the cross flow consequently, the mixing flow deflects to the upper side wall due to the recirculation zone which was formed behind the jet. Then, the pressure increases gradually to reach the reattachment point and it decreases gradually due to the friction effect. As the velocity ratio increases, the pressure increases just after the injection location. This is because the restriction of the flow increases by increasing the velocity ratio. As the velocity ratio increases, the value of the pressure behind the jet location decreases. This is because the intensity of secondary flow increases with increase the velocity ratio consequently, the pressure reduces.

5.8 Effect of jet angle on the wall pressure distributions

Figure 13 represents a graph of the wall pressure coefficient $(\overline{P}_w - \overline{p}_a / 0.5\rho U_c^2)$ as function of jet angle at constant value of the velocity ratio (R= 5.8). From this figure, it can be observed that the pressure increases by increasing the jet angle before the injection location due to the jet flow decelerates the main flow consequently, the pressure increases. After the injection position, the value of the pressure decreases by increasing the jet angle. This is because the intensity of secondary flow increases with increase of the jet angle. At the jet angle equal 90^o, the horizontal velocity components equals zero, then the effect of the vertical velocity for injection has similar effect of the flow over an obstacle. At the jet angle is less than 90^o, the jet flow

becomes horizontal velocity. As the jet angle decreases, this velocity increases then the recirculation zone decreases and the reattachment length decreases.

6. CONCULIONS

The behavior of fluid flow of steady incompressible turbulent flow for the injection into a cross flow was carried out numerically and experimentally.
The effect of the velocity ratio and the injection angle on the flow characteristics are studied. From the analysis of the results the following conclusion are obtained.

- The recirculation zone behind the jet is larger in the case of higher values of velocity ratios at constant jet angle.
- The recirculation zone generated front the jet, depends on the velocity ratio for constant jet angle .
- The reattachment length increases by increasing the velocity ratio at constant jet angle and decreases by decreasing the jet angle for constant velocity ratio
- The amplitude of the negative value of the x- component velocity in recirculation zone increases by increasing of the velocity ratio and the maximum value of this component also increases with increase the velocity ratio for constant jet angle.
- As the angle of jet decreases, the amplitude of the negative value of the x-component velocity decreases in the recirculation zone behind the jet and it becomes positive value at
  low value of jet angle.
- As the angle of jet decreases, the amplitude of the negative value of the y-component velocity decreases in the recirculation zone behind the jet and it becomes positive value in
  upper side of test section. Also it decreases by increasing of distance x/b but it increases as the velocity ratio increases
- As the velocity ratio increases, the static wall pressure increases front the jet inlet and decreases quickly in the recirculation zone which occurs behind the jet.
- The value of the static wall pressure decreases just after the inlet location of jet by decreasing the jet angle but it increases again after that.
- The comparison between the numerical results and present experimental results gives good agreement, also with measurement data [1]

References

[1] A. D. Fitt, J R. O. Ckendon and T. V. Jones, Aerodynamic of slot- film cooling, theory and experiment, J. Fluid Mechanics 16 (1985)

[2] H. Haniu and B. R. Ramaprian, Studies on two –dimensional Curved nonbuoyant jets in cross flow, ASME journal of Fluids Engineering 111 (1989) 78-86.

[3] B. R. Ramaprian, and H. Haniu , Measurments in two –dimensional plume in cross flow, ASME journal of Fluids Engineering 111 (1989) 130-138

[4] J. M. M. Barata, D. F. G. Durao, and M. V. Heitor “Velocity characteristics of
multiple impinging jets through a cross flow”, J. Fluid Eng., Vol. 114, pp. 231-239 (1992)

[5] J. M. M. Barata “Fountain flows produced by multiple impinging jets in a cross flow”, AIAA Journal, Vol. 34, No. 12 (1996)

[6] S. Sarkar and T. K. Bose, Comparison of different turbulence models for prediction of slot –film cooling flow and temperature fields, Numerical Heat Transfer Part B. 28 (1995) 217-238

[7] B. E. Launder . and D. B. Spalding, The numerical computation of turbulent flows, Computer Methods in Applied Mechanics and Engineering, 3 (1974) 269-289

[8] S. V Patankar, D. K. Basu and S. A. Alpay, Production of three –dimensional velocity field of a deflected turbulent jet, ASME journal of Fluids Engineering 99 (1977) 758-762

[9] G. D. Catalano , K. S. Chang and J.A. Mathis, Investigation of turbulent jets impingement in a confined cross flow, AIAA Journal, 27(1989) 1530-1535.

[10] G. He , Y. Guo and A. T. Hsu, The effect of Schmidt number on turbulent scalar mixing in jet-in-in crossflow, Int. Journal of Heat Mass Transfer, 42(1999) 3727-3738

[11] P. G. Kassimatis, G. C. Bergeles, T. V. Jones and J. W. Chew, Numerical investigation of the aerodynamics of the near –slot film cooling, International Journal for Numerical Methods in fluids, 32(2000) 97-117

[12] El-Gabry , L. A. and Kaminski, D. A. ," Numerical investigation of jet impingement with crassflow- comparison of Yang-Shih and standard k – ε turbulence models" Numerical Heat Transfer Part A. 47(2005) 441-469

[13]. K. Kalita, A. Dewan and A. K. Dass, Prediction of turbulent plane jet in cross flow, " Numerical Heat Transfer Part A. 41 (2002), 101-111

[14] M. A. Leschziner and W. Rodi, Calculation of annular and twin parallel jets using various discretization schemes and turbulence- model variations, ASME Fluids Eng. 103(1981)

[15] S. V. Patankar, Numerical Heat Transfer and Fluid Flow,. McGraw-Hill, New York (1980)

NOMENCLATURE

b	slot width	m
c_1,	c_2 , c_d, empirical constants of k-ε model	
Cp	pressure coefficient ($\bar{p}$ /0.5 ρU_c^2)	
H	height of cross flow section	m
k	dimensionless of turbulent kinetic energy ($\bar{k}$ / V_J^2)	
$\bar{k}$	turbulent kinetic energy	J/kg
L	lenth of the test section	m
P	dimensionless pressure	
p_w	wall static pressure	
p_a	atmospheric pressure	
$\bar{p}$	static pressure	N/m^2
R	velocity ratio (R= V_J / Uc)	
Re	Reynolds number ($Re=\rho V_J d/\mu$)	
Re_t	turbulent Reynolds number ($\underline{Re_t = \rho V_J d/\mu_t}$)	
S_{ij}	deformation rate tensor	
u	dimensionless of horizontal velocity (u = $\bar{u}$ / V_J)	
$\bar{u}$	horizontal component of local mean velocity	m/sec
v	dimensionless of vertical velocity ($v = \bar{v}/V_J$)	
$\bar{v}$	vertical velocity	m/sec

V_j average velocity at the jet injection location m/sec

x,y Cartesian coordinates

ε dimensionless of dissipation rate of k ,$(e = \bar{e}d / V_J^3)$

$\bar{\varepsilon}$ dissipation rate of k J/kg

ν kinematics viscosity m^2/s

ρ density Kg/m3

σ_ε model constant

σ_κ model constant

Subscripts

c cross flow

j jet exit`

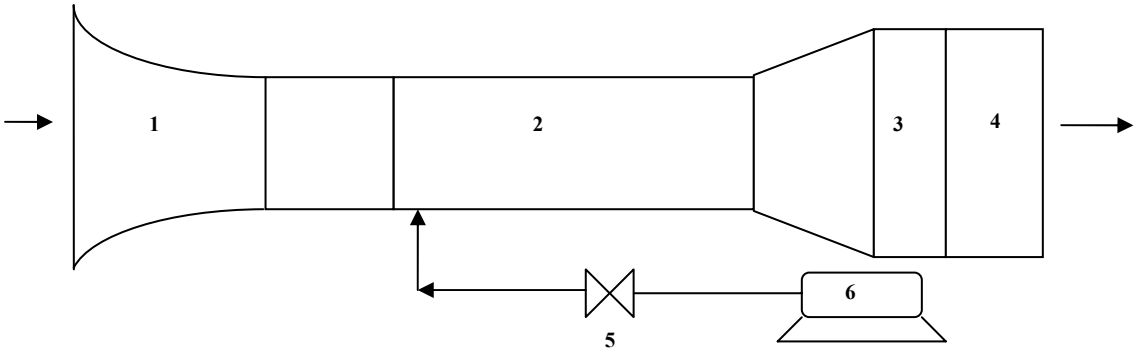

1-bell mouth 2- test section 3- diffuser 4- fan
5- control valve 6- reciprocating compressor

Fig 1a. layout of test section

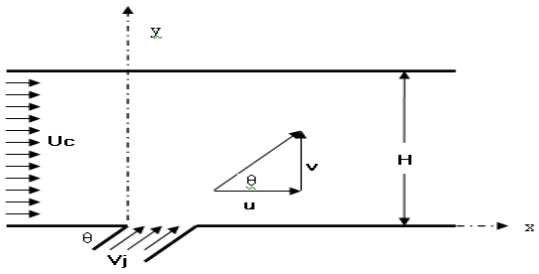

Fig. 1.b. The physical mode

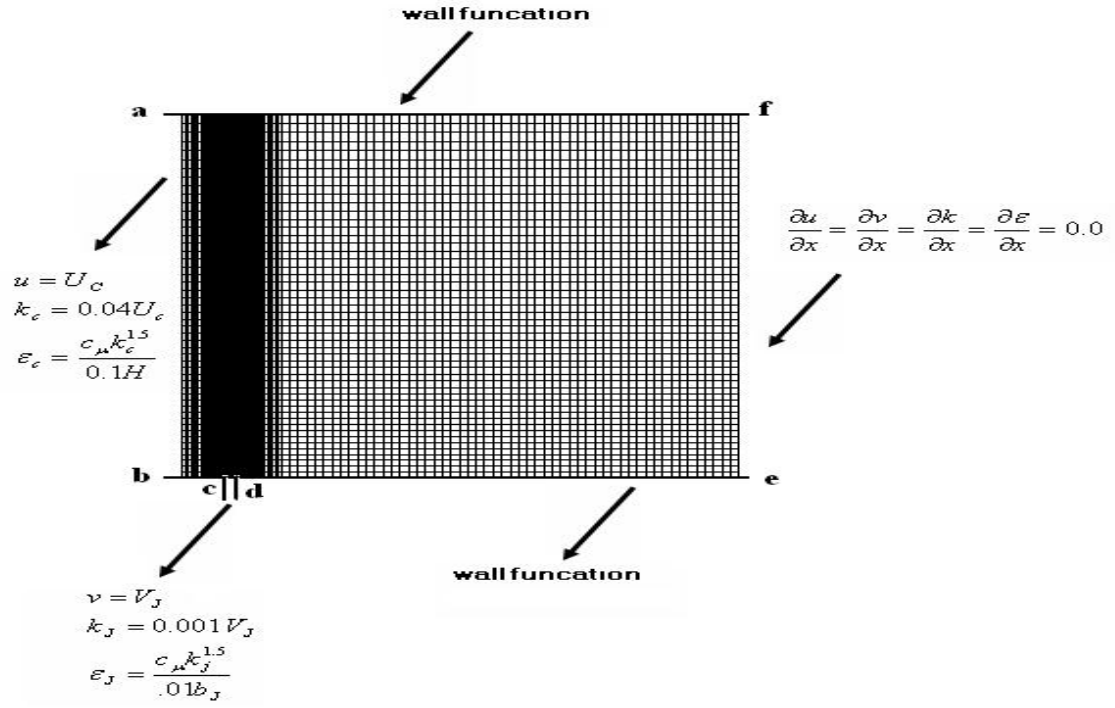

Fig. 2(a) Boundary condition for computation grid

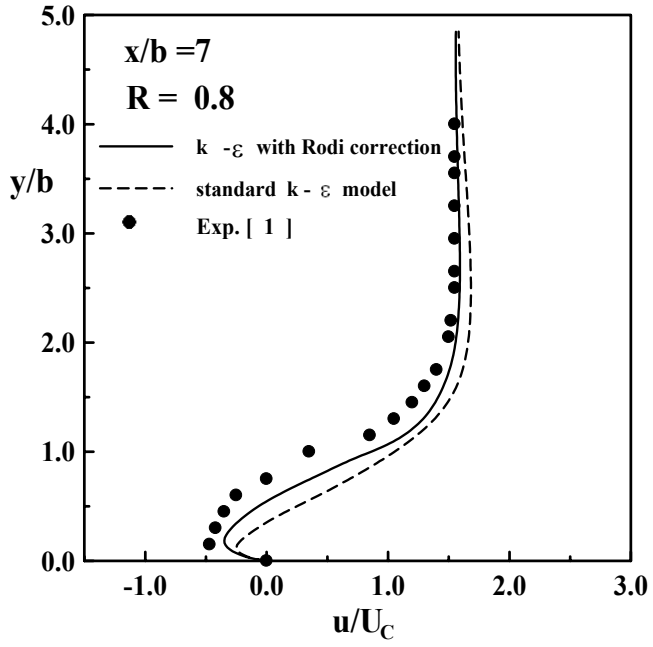

Fig. 2(b) effect the turbulence model on the x- component velocity (u/U_c)

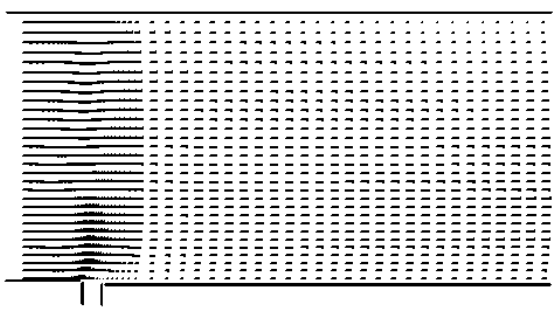

(a) R = 0.1

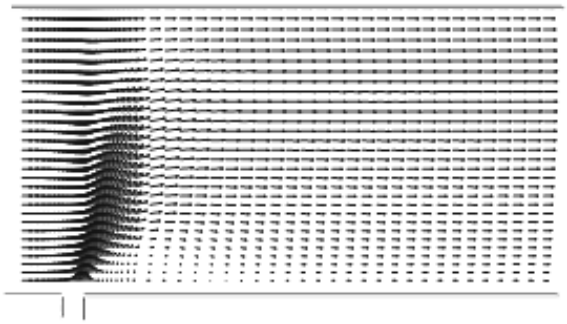

(b) R = 0.8

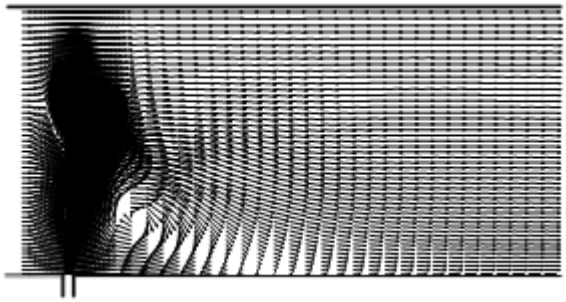

(c) R = 15.2

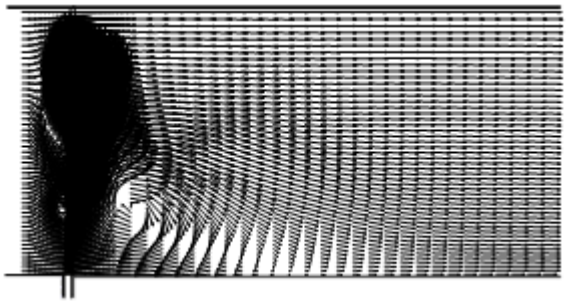

(d) R = 20.5

Figure 3 Mean velocity vectors field for different values of velocity ratio at constant jet angle, , $\theta = 90^o$

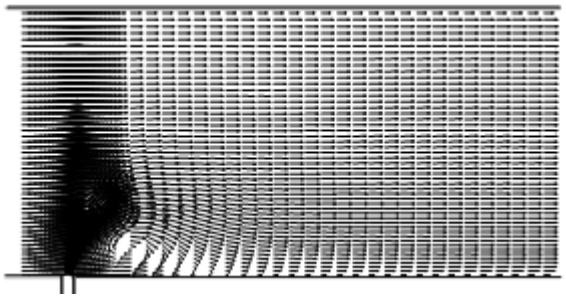

(a) $\theta = 90^o$

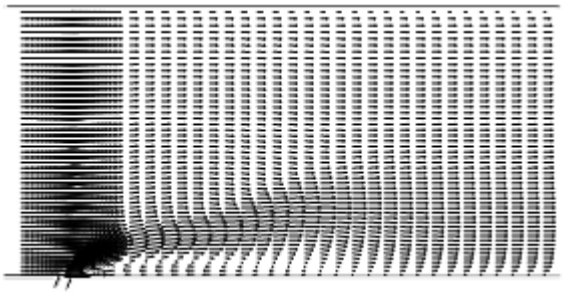

(b) $\theta = 60^o$

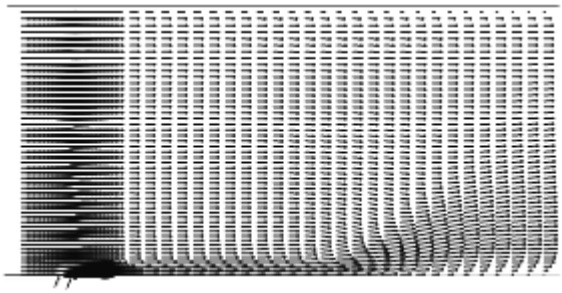

(c) $\theta = 30^o$

Figure 4 Mean velocity vectors field for different values of jet angle at velocity ratio, R = 5.8

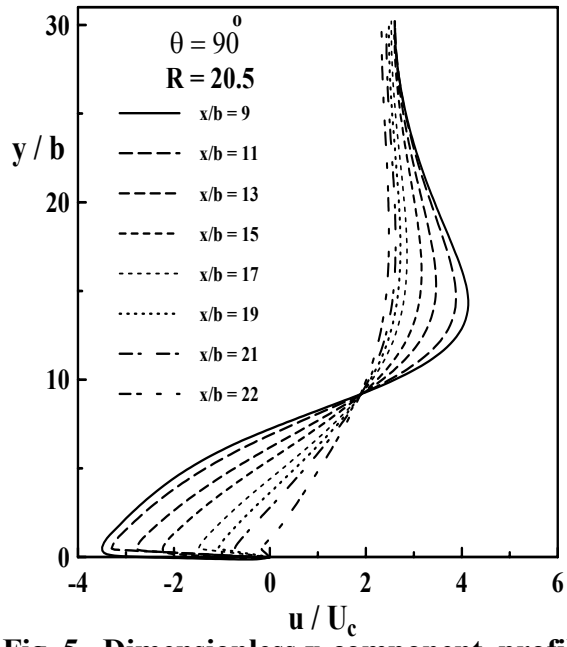

Fig. 5 Dimensionless x-component profile $u/U_c(y/b)$ at different distances x/b , θ=90 ° ,R=20.5

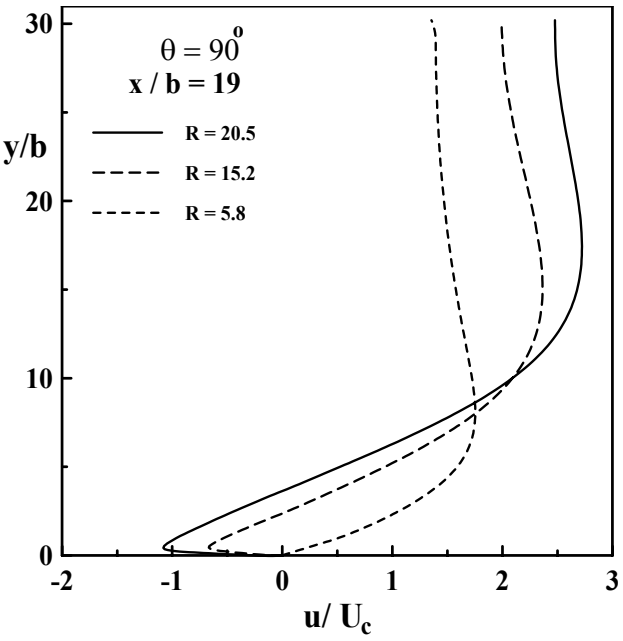

Fig. 6 Dimensionless x-component profile $u/U_c(y/b)$ at three velocity ratios (R) θ=90 °, x/b=19

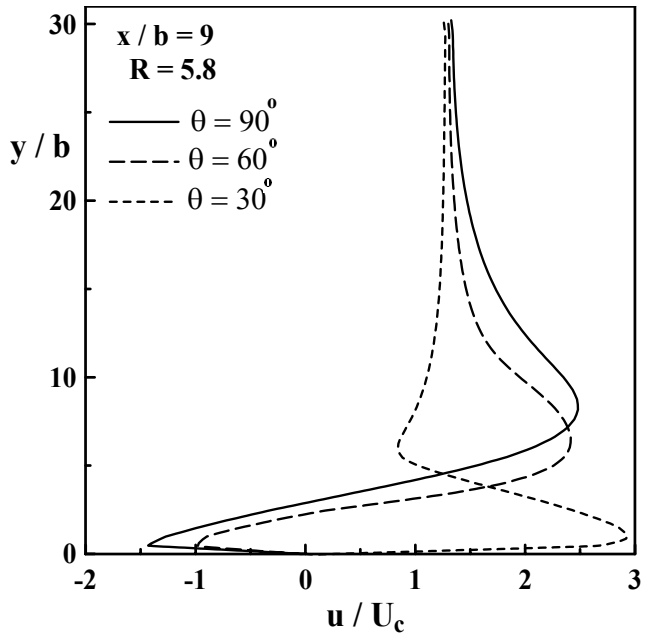

Fig. 7 Dimensionless x-component profile (u/Uc)(y/b) for 3-different jet angle (θ),x/b=9 , R=5.8

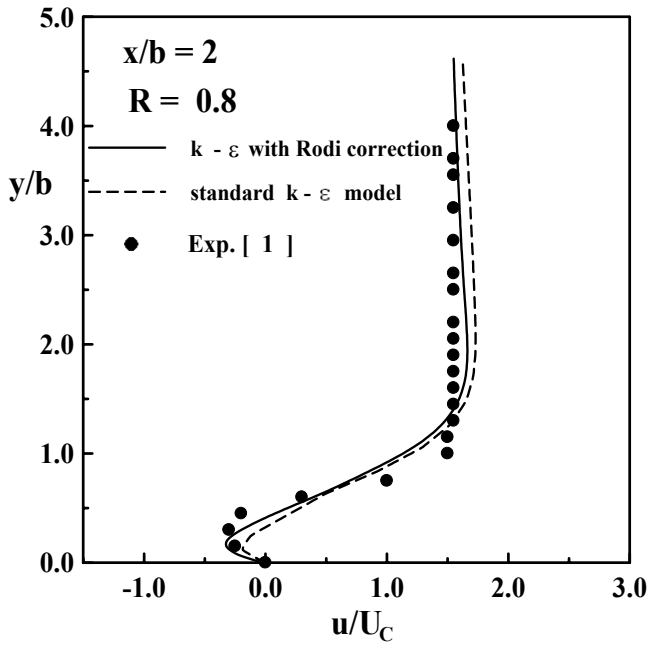

Fig. 8(a)

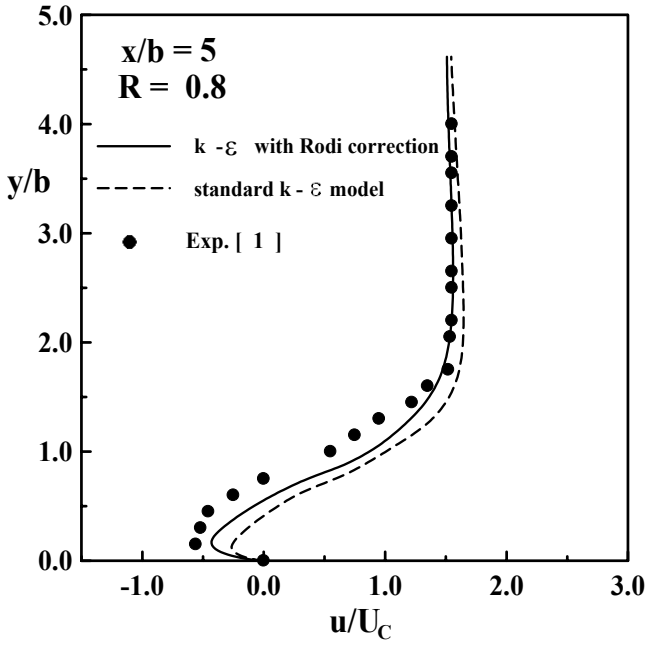

Fig. 8(b)

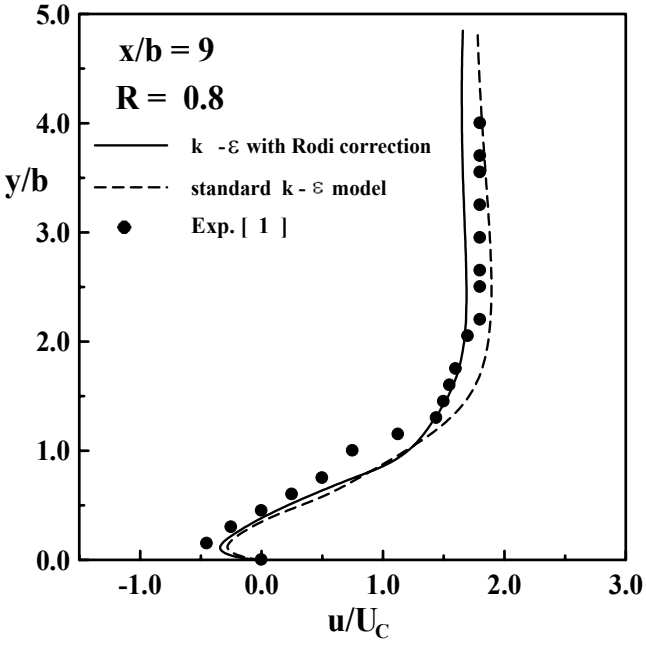

Fig. 8(c)

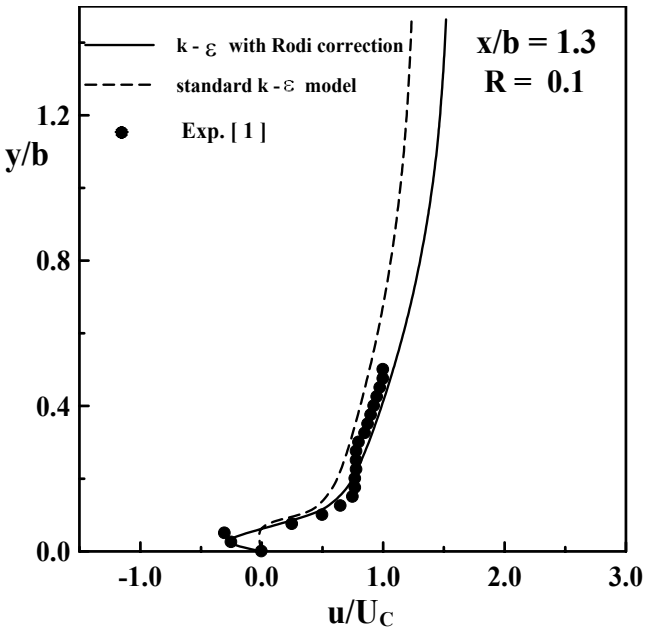

Fig. 8(d)

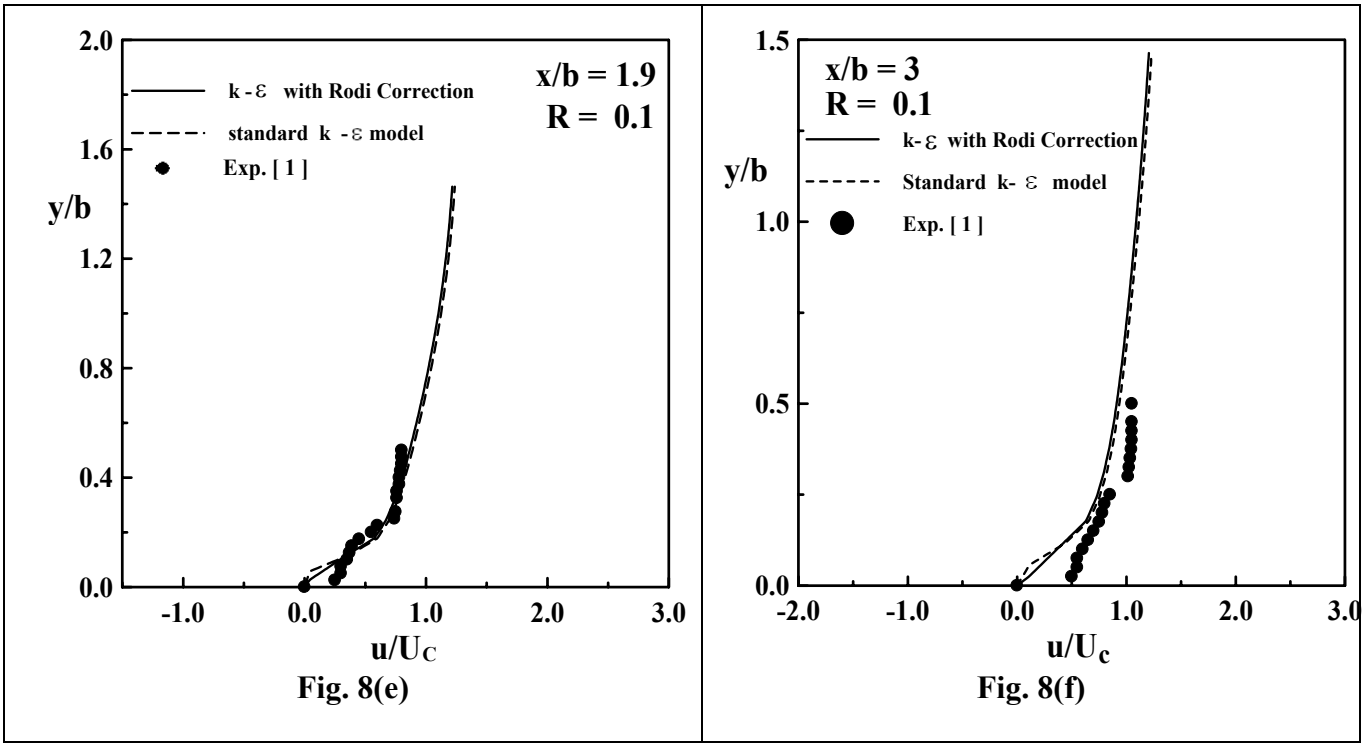

Fig. 8(e) Fig. 8(f)

Fig. 8 Effect of the turbulence model x-component velocity (u/U_c)

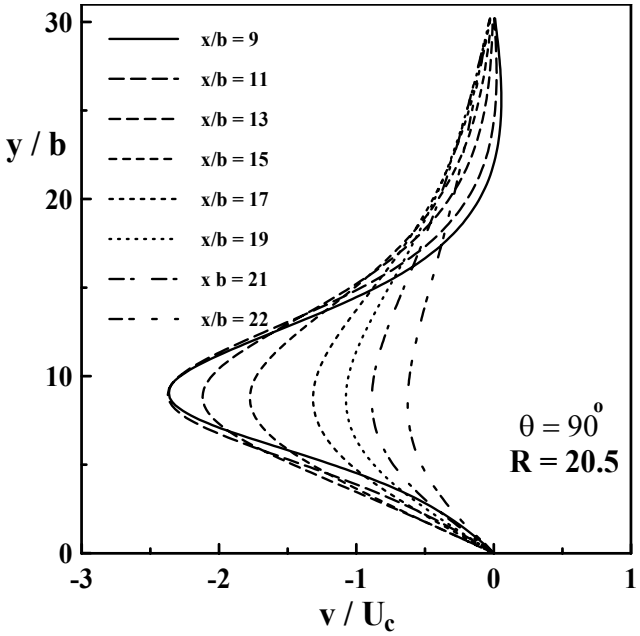

Fig. 9 Dimensionless y-component profile (v/Uc)(y/b) at different values of distance jet x/b , θ, R=20.8

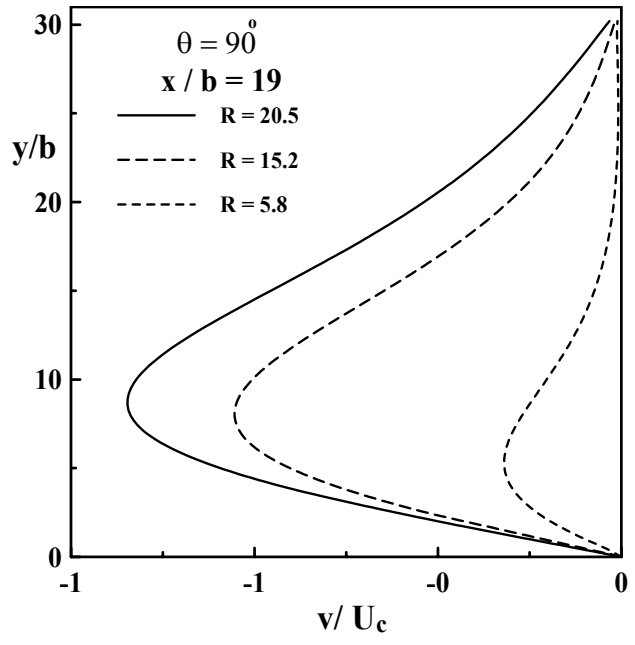

Fig.10 Dimensionless y-component velocity profile (v/Uc)(y/b) at 3- different velocity ratio (R) , θ=90°, x/b =19

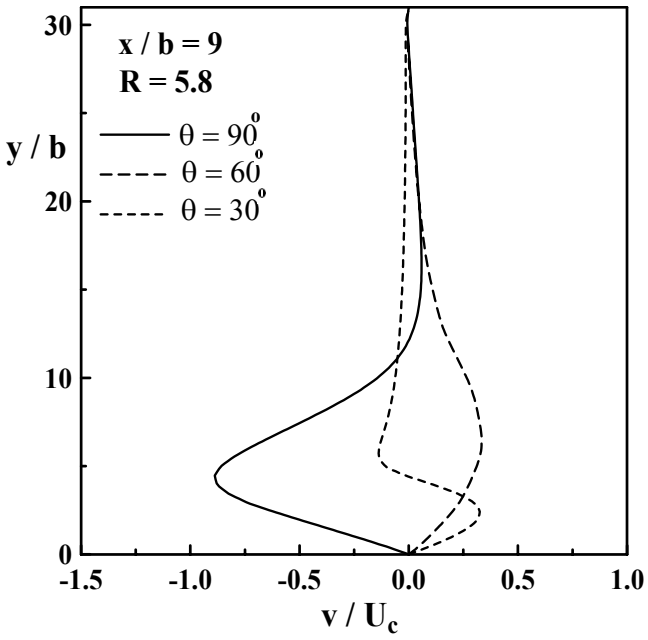

Fig.11 Dimensionless y-component velocity profile (v/Uc)(y/b) for 3- different jet angles (θ) , R=5.8, x/b =9.

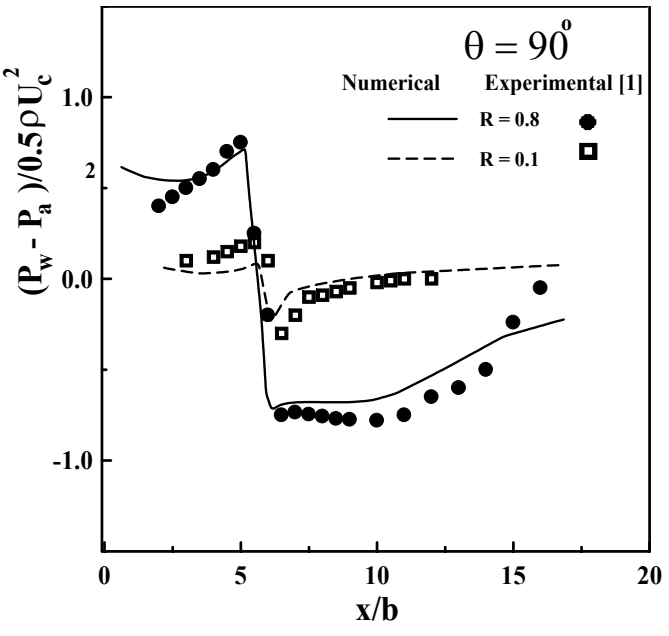

Fig.12(a)

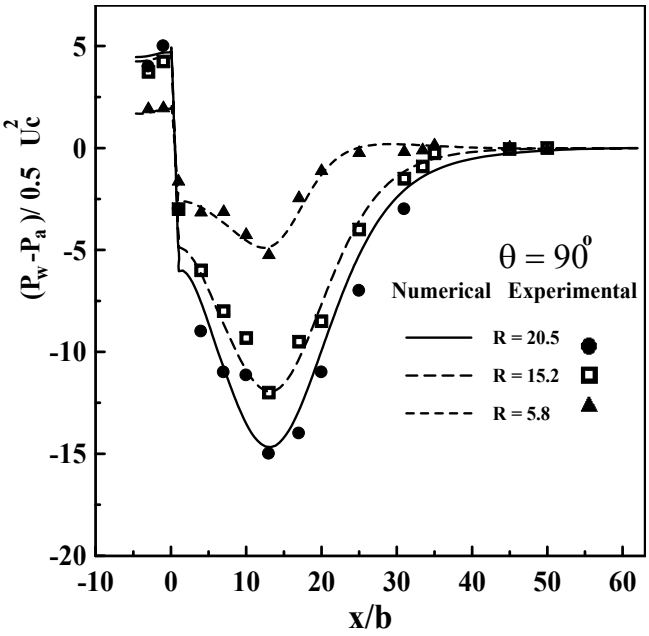

Fig.12(b)

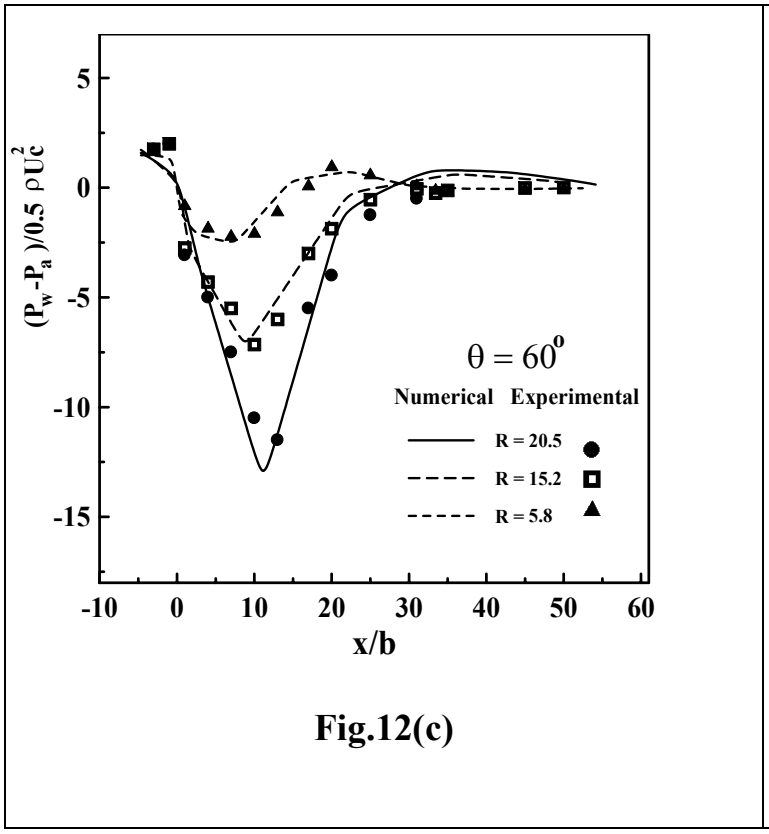

Fig.12(c)

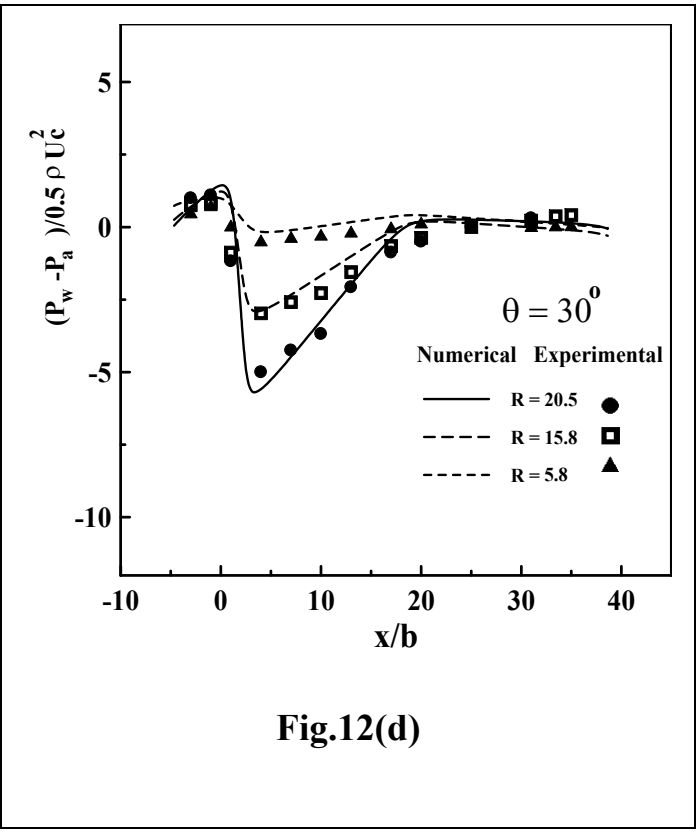

Fig.12(d)

Fig. 12 Comparison between measured and computed wall pressure for three different velocity ratios at
(a) & (b) θ = 90°,(c) θ = 60° and (d) θ = 30°

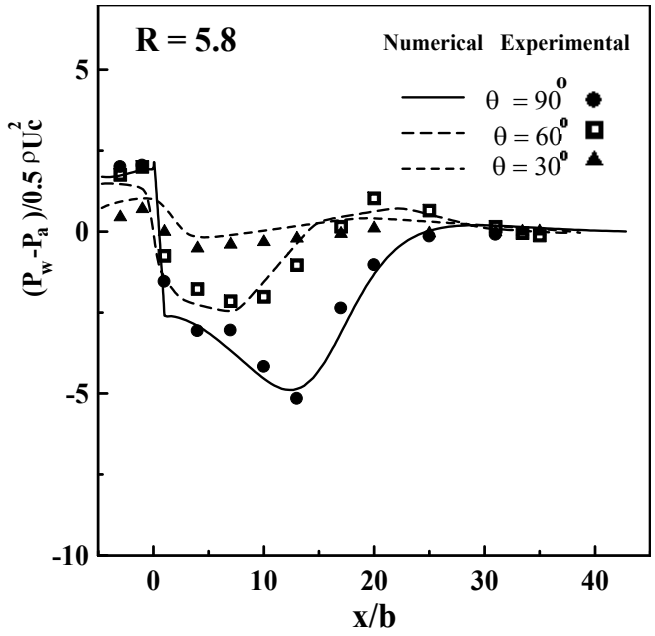

Fig. 13 Comparison between measured and the numerically computed wall pressure at three different values of jet angles, R=5.8